Non-Hermitian Chern Bands

Shunyu Yao,[1] Fei Song,[1] and Zhong Wang[1,2,*]
[1]Institute for Advanced Study, Tsinghua University, Beijing 100084, China
[2]Collaborative Innovation Center of Quantum Matter, Beijing 100871, China

(Received 15 April 2018; revised manuscript received 14 June 2018; published 24 September 2018)

The relation between chiral edge modes and bulk Chern numbers of quantum Hall insulators is a paradigmatic example of bulk-boundary correspondence. We show that the chiral edge modes are not strictly tied to the Chern numbers defined by a non-Hermitian Bloch Hamiltonian. This breakdown of conventional bulk-boundary correspondence stems from the non-Bloch-wave behavior of eigenstates (non-Hermitian skin effect), which generates pronounced deviations of phase diagrams from the Bloch theory. We introduce non-Bloch Chern numbers that faithfully predict the numbers of chiral edge modes. The theory is backed up by the open-boundary energy spectra, dynamics, and phase diagram of representative lattice models. Our results highlight a unique feature of non-Hermitian bands and suggest a non-Bloch framework to characterize their topology.

DOI: 10.1103/PhysRevLett.121.136802

Hamiltonians are Hermitian in standard quantum mechanics. Nevertheless, non-Hermitian Hamiltonians [1,2] are highly useful in describing many phenomena such as various open systems [3–12] and waves propagations with gain and loss [13–39]. Recently, topological phenomena in non-Hermitian systems have attracted considerable attention. For example, an electron's non-Hermitian self-energy stemming from disorder scatterings or electron-electron interactions [40–42] can generate novel topological effects such as bulk Fermi arcs connecting exceptional points [40,41] (a photonic counterpart has been observed experimentally [43]). The interplay between non-Hermiticity and topology has been a growing field with a host of interesting theoretical [44–75] and experimental [76–82] progresses witnessed in recent years.

A central principle of topological states is the bulk-boundary (or bulk-edge) correspondence, which asserts that the robust boundary states are tied to the bulk topological invariants. Within the band theory, the bulk topological invariants are defined using the Bloch Hamiltonian [83–86]. This has been well understood in the usual context of Hermitian Hamiltonians; nevertheless, it is a subtle issue to generalize this correspondence to non-Hermitian systems [44–48,53–56]. As demonstrated numerically [46,53,54,56], the bulk spectra of one-dimensional (1D) open-boundary systems dramatically differ from those with periodic boundary condition, suggesting a breakdown of bulk-boundary correspondence. This issue has been resolved [56] in 1D non-Hermitian Su-Schrieffer-Heeger (SSH) model: the topological end modes are determined by the non-Bloch winding number [56] instead of topological invariants defined by Bloch Hamiltonian [45–52], which suggests a generalized bulk-boundary correspondence [56].

However, the general implications of these results based solely on a simple 1D model remain to be understood (e.g., is the physics specific to 1D?). Moreover, the topology of this 1D model requires a chiral symmetry [85], which is often fragile in real systems. Thus, we are motivated to study 2D non-Hermitian Chern insulators whose robustness is independent of symmetries [87–90]. In addition, non-Hermitian Chern bands are relevant to a number of physical systems (e.g., photonic Chern insulators [37] with gain or loss, topological-insulator lasers [75,91], interacting or disordered electron systems [40]). They have been characterized by non-Hermitian generalizations of Bloch Chern numbers [44,45], which are expected to predict the edge states.

In this Letter, we uncover an unexpected bulk-boundary correspondence of non-Hermitian Chern bands. We find that the chiral edge states are not strictly related to the Chern numbers of non-Hermitian Bloch Hamiltonians. More remarkably, in spite of this breakdown of conventional bulk-boundary correspondence, the edge states retain a general topological characterization. In fact, the "breakdown" stems from the general non-Bloch-wave behavior of eigenstates (non-Hermitian skin effect), which affects the phase diagrams in a dramatic yet predictable manner. We therefore introduce "non-Bloch Chern numbers" to which the numbers of chiral edge modes are strictly tied. Notably, complex-valued wave vector (momentum) is used in their construction, which captures a unique feature of non-Hermitian bands. As an illustration, we study a concrete lattice model, whose energy spectra, dynamics (edge wave propagations), and phase diagram are found to be in accordance with our theory.

Bloch Hamiltonian.—We consider a lattice model similar to that of Ref. [44]. The Bloch Hamiltonian is

$$H(\mathbf{k}) = (v_x \sin k_x + i\gamma_x)\sigma_x + (v_y \sin k_y + i\gamma_y)\sigma_y + (m - t_x \cos k_x - t_y \cos k_y + i\gamma_z)\sigma_z, \quad (1)$$

where $\sigma_{x,y,z}$ are Pauli matrices. The Hermitian part is the Qi-Wu-Zhang model [92] (a variation of Haldane model [88]); the non-Hermitian parameters $\gamma_{x,y,z}$ appear as "imaginary Zeeman fields" [93]. When $\gamma_{x,y,z} = 0$, the model has a topological transition at $m = t_x + t_y$, where the Chern number jumps. We shall focus on m being close to $t_x + t_y$ ($\gamma_{x,y,z}$ are taken to be small compared to $t_{x,y}$). The eigenvalues of $H(\mathbf{k})$ are

$$E_\pm(\mathbf{k}) = \pm\sqrt{\sum_{j=x,y,z}(h_j^2 - \gamma_j^2 + 2i\gamma_j h_j)}, \quad (2)$$

where $(h_x, h_y, h_z) = (v_x \sin k_x, v_y \sin k_y, m - \sum_j t_j \cos k_j)$.

A band is called "gapped" or "separable" [44] if its energies in the complex plane are separated from those of other bands. In this model, the Bloch bands are gapped if $E_\pm(\mathbf{k}) \neq 0$. The gapped regions are found to be $m > m_+$ and $m < m_-$, where $m_\pm$ have simple expressions when $\gamma_z = 0$

$$m_\pm = t_x + t_y \pm \sqrt{\gamma_x^2 + \gamma_y^2}. \quad (3)$$

The Bloch phase boundaries are $m = m_\pm$, where the gap closes at $\mathbf{k} = (0, 0)$. One can obtain that the $H(\mathbf{k})$-based Chern number (Bloch Chern number) [44,45] is 0 for $m > m_+$, 1 for $m < m_-$, and becomes nondefinable in the gapless region $m \in [m_-, m_+]$.

Open boundary.—According to the usual bulk-boundary-correspondence scenario, the chiral edge states of an open-boundary system should be determined by the Bloch Chern numbers. However, a different physical picture is found here. Let us present numerical results before the theory. To be concrete, let us take $\gamma_z = 0$ and focus on the x-y-symmetric cases, namely $v_x = v_y = v$, $t_x = t_y = t$, $\gamma_x = \gamma_y = \gamma$. We fix $v = t = 1$ and solve the real-space lattice Hamiltonian on a square geometry with edge length L in both x and y directions, taking (m, γ) as the varied parameters. Among other results we find:

(i) The open-boundary spectra are prominently different from those of Bloch Hamiltonian. Although the Bloch spectra are complex valued [see Eq. (2)], the majority of square-geometry energy eigenvalues are real valued when $\gamma_z = 0$. It should be mentioned that the reality of open-boundary spectra is not a general rule; in other models, they are often complex (e.g., when γ_z is nonzero); nevertheless, in general the open-boundary and Bloch spectra have pronounced differences.

The reality of square-geometry spectra can be explained as follows. To avoid lengthy notations, we simply take $L = 2$ as an illustration. Let us order the four sites as $(x, y) = (1, 1), (2, 1), (1, 2), (2, 2)$, then the real-space Hamiltonian reads

$$H = \begin{pmatrix} M & T_x & T_y & 0 \\ T_x^\dagger & M & 0 & T_y \\ T_y^\dagger & 0 & M & T_x \\ 0 & T_y^\dagger & T_x^\dagger & M \end{pmatrix}, \quad (4)$$

where

$$M = m\sigma_z + i\gamma_x\sigma_x + i\gamma_y\sigma_y,$$
$$T_x = -\frac{t_x}{2}\sigma_z - i\frac{v_x}{2}\sigma_x, \qquad T_y = -\frac{t_y}{2}\sigma_z - i\frac{v_y}{2}\sigma_y. \quad (5)$$

This Hamiltonian is "η-pseudo-Hermitian" [94,95] (not PT-symmetric [38,58]), namely, it satisfies $\eta^{-1}H^\dagger\eta = H$, where η is the direct product of spatial inversion and σ_z:

$$\eta = \begin{pmatrix} 0 & 0 & 0 & \sigma_z \\ 0 & 0 & \sigma_z & 0 \\ 0 & \sigma_z & 0 & 0 \\ \sigma_z & 0 & 0 & 0 \end{pmatrix}. \quad (6)$$

The pseudo-Hermiticity guarantees that from $H|\psi_n\rangle = E_n|\psi_n\rangle$, one can infer $E_n\langle\psi_n|\eta|\psi_n\rangle = E_n^*\langle\psi_n|\eta|\psi_n\rangle$, which means $E_n = E_n^*$ when $\langle\psi_n|\eta|\psi_n\rangle \neq 0$. In this model, we find that the majority of eigenstates have $\langle\psi_n|\eta|\psi_n\rangle \neq 0$ in the relevant region of parameter space.

The dissimilarity between open-boundary and Bloch spectra has also been found in a 1D model [46,53,54,56], whose spectra can be readily obtained via a similarity transformation to a Hermitian Hamiltonian [56]. Free of this specificity, our 2D model is a more nontrivial and representative exemplification of the phenomenon that the open-boundary spectra are noticeably different from the Bloch spectra.

(ii) The topological transition between nontrivial and trivial phases (i.e., with and without robust chiral edge modes) does not occur at the Bloch phase boundary $m = m_\pm$ [Eq. (3)]. By numerically scanning the gap-closing points [96], we find that the phase boundary is a single curve (red solid one in Fig. 1), in sharp contrast to the two straight lines $m = m_\pm$ obtained from the Bloch Hamiltonian. Furthermore, the numerical phase boundary can be well approximated by the theoretical prediction of Eq. (14).

As an illustration of the phase diagram, we show in Fig. 2 the numerical spectra for two values of parameters indicated as filled square and asterisk in Fig. 1. Both filled square and asterisk are taken at the Bloch phase boundary where the Bloch Hamiltonian is gapless. Remarkably, the spectra at filled square clearly display an energy gap ≈ 0.4 [Fig. 2(a), left panel]. A similar bulk gap is found for the

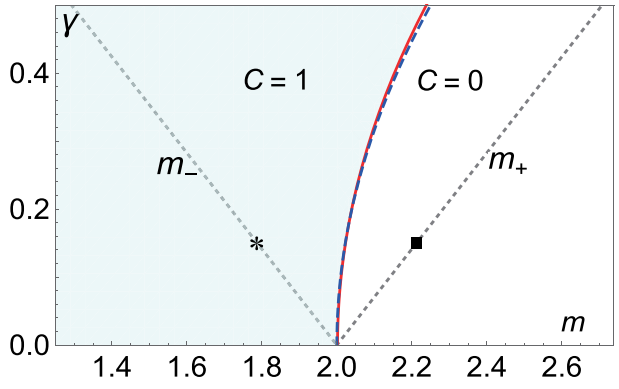

FIG. 1. Topological phase diagram based on open-boundary spectra (for $v_{x,y} = t_{x,y} = 1, \gamma_{x,y} = \gamma, \gamma_z = 0$). Chiral edge states are found in the shadow area, which is therefore topologically nontrivial. The trivial-nontrivial phase boundary (red solid curve) is well approximated by the theoretical curve in Eq. (14) (shown as the blue dashed curve, which is very close to the red solid curve). Away from this phase boundary, the (open-boundary) bulk spectra are gapped. The Bloch-Hamiltonian phase boundaries are shown as the dotted lines, whose equations are $m = m_{\pm}$ with $m_{\pm} = 2 \pm \sqrt{2}\gamma$. The Bloch spectra are gapless in the fan $m \in [m_-, m_+]$. The non-Bloch Chern number C is defined in Eq. (13) (we take the $\mathrm{Re}(E_\alpha) < 0$ band and omit the α index; see text).

asterisk point; in addition, there are a few in-gap energies, which can be identified as those of chiral edge modes. The absence or existence of chiral edge modes can also be detected by wave-packet motions (Fig. 2, right panels). In Fig. 2(a), there are no chiral edge modes, and the initial wave functions are superpositions of bulk eigenstates; therefore, the wave packet quickly enters the bulk; in Fig. 2(b), one can see clear signatures of chiral motions along the edge.

Finally, we emphasize that the phase diagram is independent of the geometry of system, which indicates its topological nature. For example, the disk geometry $(x^2 + y^2 \le R^2)$ produces the same phase diagram as Fig. 1 (see the Supplemental Material [97]).

Non-Bloch Chern number.—This intriguing phase diagram is a prediction of the non-Bloch theory based on complex-valued wave vectors. We now introduce this formulation. First, we find that all the bulk eigenstates are exponentially localized at the boundary of system [98,99]. This "non-Hermitian skin effect" [56] is possible because the eigenstates are nonorthogonal. To see this effect explicitly, we consider the low-energy continuum model of Eq. (1) (with $\gamma_z = 0$), which is its expansion to the k_j^2 order:

$$H(\mathbf{k}) = (v_x k_x + i\gamma_x)\sigma_x + (v_y k_y + i\gamma_y)\sigma_y + \left(m - t_x - t_y + \frac{t_x}{2}k_x^2 + \frac{t_y}{2}k_y^2\right)\sigma_z. \quad (7)$$

It can be decomposed as $H(\mathbf{k}) = H_0 + H_1$, where $H_1 = i\gamma_x\sigma_x + i\gamma_y\sigma_y$, and H_0 is the rest part. For small $\mathbf{k}$, we have $\partial H_0/\partial k_j = v_j\sigma_j$ and $H_1 = i\sum_{j=x,y}(\gamma_j/v_j)(\partial H_0/\partial k_j) = \sum_j(\gamma_j/v_j)[x_j, H_0]$, where $(x_x, x_y) \equiv (x, y)$. Note that $x_j = i(\partial/\partial k_j)$ in the $\mathbf{k}$-space representation. Let us treat H_1 as a perturbation. The lowest-order perturbation to an

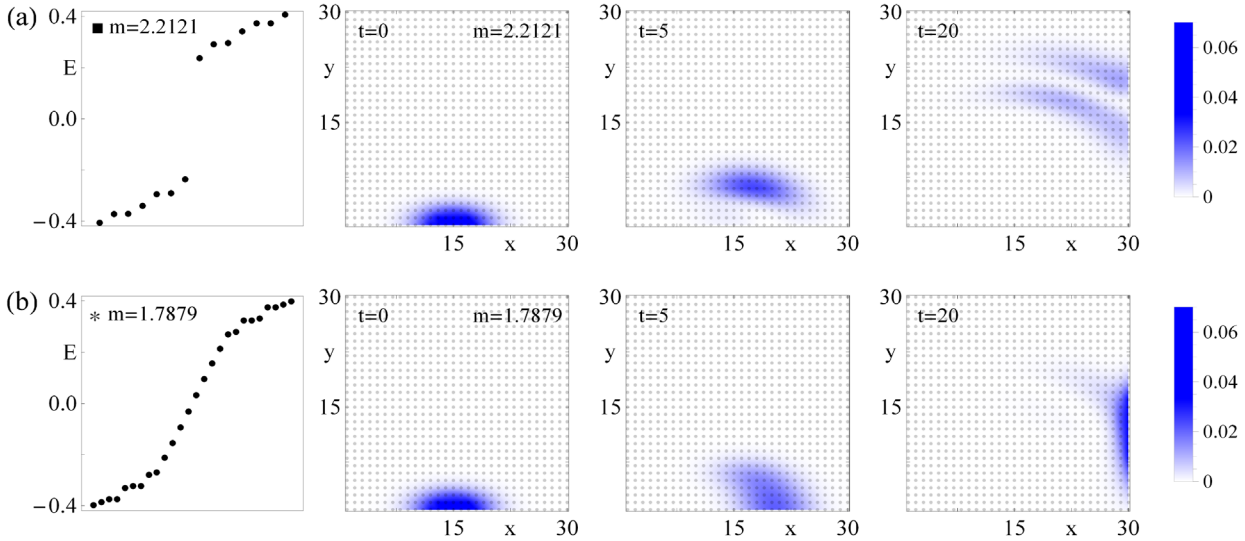

FIG. 2. Left panel: Lowest energy eigenvalues of a square geometry with $L = 30$. Right three panels: wave-packet evolutions. (a) $m = 2.2121$; (b) $m = 1.7879$ (indicated by filled square and asterisk in Fig. 1), with $\gamma = 0.15$ for both. The energy eigenvalues shown here are real valued. In (a), a nonzero energy gap is apparent and in (b), there are a few in-gap energies of chiral edge states. For the wave-packet evolution, the initial state takes the Gaussian form $\psi(t = 0) = \mathcal{N}\exp[-(x - 15)^2/40 - (y - 1)^2/10](1, 1)^T$, $\mathcal{N}$ being the normalization factor, and evolves according to the Schrodinger equation $i\partial_t|\psi(t)\rangle = H|\psi(t)\rangle$. The intensity profile of $|\psi(t)\rangle$ (modulus squared), normalized so that the total intensity is 1, is shown for $t = 0, 5, 20$. The wave packet quickly fades into the bulk in (a), whereas the chiral (unidirectional) edge motion is appreciable in (b).

eigenstate $|n\rangle$ of H_0 is $\sum_{l\neq n}|l\rangle\langle l|H_1|n\rangle/(E_n-E_l)=\sum_{l\neq n}\sum_j(\gamma_j/v_j)|l\rangle\langle l|x_j|n\rangle=\sum_j(\gamma_j/v_j)(x_j-\bar{x}_j)|n\rangle$, where $\bar{x}_j\equiv\langle n|x_j|n\rangle$. Therefore, the associated eigenstate of H is $|\psi_n\rangle=[1+\sum_j(\gamma_j/v_j)(x_j-\bar{x}_j)]|n\rangle\approx\exp[\sum_j(\gamma_j/v_j)\times(x_j-\bar{x}_j)]|n\rangle$. Thus, for an extended state $|n\rangle$, $|\psi_n\rangle$ is exponentially localized like $\exp[(\gamma_x/v_x)x+(\gamma_y/v_y)y]$ [100]. The role of non-Hermiticity is notable in this derivation: without the "i" factor in H_1, we would have obtained a phase factor instead of exponential decay.

In view of this non-Hermitian skin effect, we take a complex-valued wave vector (or momentum) to describe open-boundary eigenstates:

$$\mathbf{k}\to\tilde{\mathbf{k}}+i\tilde{\mathbf{k}}', \tag{8}$$

where the imaginary part $\tilde{\mathbf{k}}'$ takes the simple form $\tilde{k}'_j=-\gamma_j/v_j$ for small $\tilde{\mathbf{k}}$ in this model. Accordingly, we define a "non-Bloch Hamiltonian" as follows:

$$\tilde{H}(\tilde{\mathbf{k}})\equiv H(\mathbf{k}\to\tilde{\mathbf{k}}+i\tilde{\mathbf{k}}'). \tag{9}$$

In our model, the replacement $k_j\to\tilde{k}_j-i\gamma_j/v_j$ leads to

$$\tilde{H}(\tilde{\mathbf{k}})=v_x\tilde{k}_x\sigma_x+v_y\tilde{k}_y\sigma_y+\left(\tilde{m}+\frac{t_x\tilde{k}_x^2+t_y\tilde{k}_y^2}{2}-i\sum_j\frac{t_j\gamma_j\tilde{k}_j}{v_j}\right)\sigma_z, \tag{10}$$

where

$$\tilde{m}=m-t_x-t_y-\frac{t_x\gamma_x^2}{2v_x^2}-\frac{t_y\gamma_y^2}{2v_y^2}. \tag{11}$$

The above approach toward $\tilde{H}(\tilde{\mathbf{k}})$ is quite general and can in principle be implemented directly on lattice models without taking continuum limit. Equations (8) and (9) remain applicable, though $\tilde{\mathbf{k}}'$ in general should be treated as a function of $\tilde{\mathbf{k}}$, which parametrizes a generalized Brillouin zone $\tilde{T}^2(\tilde{\mathbf{k}})$. It is a deformation of the standard Brillouin zone $T^2(\mathbf{k})$ into complex spaces.

Our non-Bloch Chern number is defined as the standard Chern number of $\tilde{H}(\tilde{\mathbf{k}})$ (not of $H(\mathbf{k})$ [44,45]). Because $\tilde{H}(\tilde{\mathbf{k}})$ is generally non-Hermitian, we define the standard right or left eigenvectors by

$$\tilde{H}(\tilde{\mathbf{k}})|u_{R\alpha}\rangle=E_\alpha|u_{R\alpha}\rangle,\qquad \tilde{H}^\dagger(\tilde{\mathbf{k}})|u_{L\alpha}\rangle=E_\alpha^*|u_{L\alpha}\rangle, \tag{12}$$

where α is the band index. The normalization $\langle u_{L\alpha}|u_{R\alpha}\rangle=1$ is required in defining Chern numbers. If we diagonalize $\tilde{H}(\tilde{\mathbf{k}})=VJV^{-1}$, J being diagonal, then every column of V [or $(V^\dagger)^{-1}$] is a right (or left) eigenvector, with the normalization $\langle u_{L\alpha}|u_{R\beta}\rangle=\delta_{\alpha\beta}$ satisfied. Now, we introduce the non-Bloch Chern number in the generalized Brillouin zone $\tilde{T}^2(\tilde{\mathbf{k}})$

$$C_{(\alpha)}=\frac{1}{2\pi i}\int_{\tilde{T}^2}d^2\tilde{\mathbf{k}}\epsilon^{ij}\langle\partial_i u_{L\alpha}(\tilde{\mathbf{k}})|\partial_j u_{R\alpha}(\tilde{\mathbf{k}})\rangle, \tag{13}$$

where $\epsilon^{xy}=-\epsilon^{yx}=1$. Equation (13) determines the chiral edge modes of open-boundary systems (squares, disks, triangles, etc.). It can also be expressed as $C_{(\alpha)}=(1/2\pi i)\int_{\tilde{T}^2}d^2\tilde{\mathbf{k}}\epsilon^{ij}\mathrm{Tr}(P_\alpha\partial_i P_\alpha\partial_j P_\alpha)$, where the projection operator $P_\alpha(\tilde{\mathbf{k}})=|u_{R\alpha}(\tilde{\mathbf{k}})\rangle\langle u_{L\alpha}(\tilde{\mathbf{k}})|$.

For the present two-band model, we shall focus on the Chern number of the "valence band" [$\mathrm{Re}(E_\alpha)<0$], omitting the α index in Eq. (13). We compute the Chern number from Eq. (10), and obtain that $C=1$ (0) for $\tilde{m}<0$ (>0). When $t_{x,y}=v_{x,y}=1,\gamma_{x,y}=\gamma$, the topologically-nontrivial condition $\tilde{m}<0$ becomes $m<2+\gamma^2$, and the phase boundary is

$$m=2+\gamma^2, \tag{14}$$

which is confirmed by our numerical calculations (see Fig. 1). We note that in the low-energy theory, γ is treated as being small, and we can see from Fig. 1 that $\gamma\sim0.5$ remains well described. As a comparison, the Bloch Chern number [44,45] is nonzero only when $m<2-\sqrt{2}\gamma$; moreover, the Bloch Chern number cannot be defined for $m\in[2-\sqrt{2}\gamma,2+\sqrt{2}\gamma]$ because the bands are gapless (inseparable).

To summarize our approach: we calculate the imaginary part $\tilde{\mathbf{k}}'$ of wave vector, which is then used to generate $\tilde{H}(\tilde{\mathbf{k}})$. The non-Bloch Chern number is then defined via $\tilde{H}(\tilde{\mathbf{k}})$ in a standard manner. The calculation is simplified in the continuum-model approach, which does not require any numerical input. For certain models, we have calculated the non-Bloch Chern number directly from the lattice models [101]. It will be useful to develop efficient algorithms to calculate $\tilde{\mathbf{k}}'$ and C beyond the continuum approach, which is left to future studies.

Cylinder.—Now we briefly discuss the cylinder topology whose spectra are noticeably different from the square or disk topology. Suppose that the cylinder has periodic-boundary condition in the x direction and open boundaries in the y direction. The Hamiltonian can be diagonalized as a family of 1D Hamiltonians parametrized by the good quantum number k_x. As an illustration, we take a set of parameters indicated as asterisk in Fig. 3(a) and show the numerical spectra in Fig. 3(b). Topological edge states can be readily seen in the spectra.

In fact, to characterize the chiral edge states on the cylinder, one can define a non-Bloch "cylinder Chern number," which is denoted as C_y for the open boundaries in y direction. The definition is quite similar to Eq. (13), except that $(\tilde{k}_x,\tilde{k}_y)$ is replaced by $(k_x,\tilde{k}_y)$, because the eigenstates are forced to be Bloch waves in the x direction. A non-Bloch "cylinder Hamiltonian" $\tilde{H}_y(k_x,\tilde{k}_y)$ can be obtained from $H(\mathbf{k})$ via $k_y\to\tilde{k}_y+i\tilde{k}'_y$ [similar to Eq. (9)], then C_y can be defined by $\tilde{H}_y$, which we shall not repeat due to the resemblance to the construction of C [Eq. (13)].

We would like to emphasize the following: (i) The value of non-Bloch cylinder Chern number depends on the edge

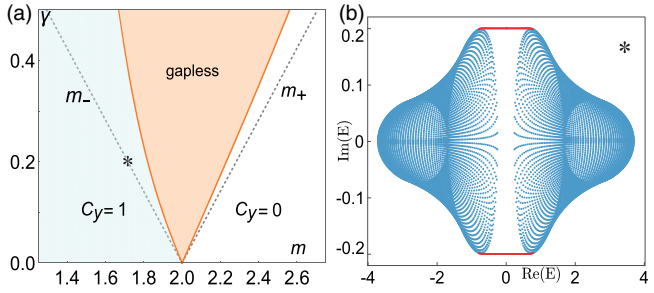

FIG. 3. (a) Phase diagram based on the spectra on a cylinder with open boundary condition in the y direction. $t_{x,y} = v_{x,y} = 1$, $\gamma_{x,y} = \gamma, \gamma_z = 0$. The dotted lines are the Bloch phase boundaries. (b) The spectra for $(m, \gamma) = (1.717, 0.2)$ (indicated as asterisk in (a)). The cylinder height is $L_y = 40$, and 180 grid points are taken for k_x. The spectra for all k_x's are shown together in the complex plane, without specifying the k_x values. The chiral edge states are shown in red.

orientation. For example, if we take open boundaries in the x direction, the Chern number C_x defined by $\tilde{H}_x(\tilde{k}_x, k_y)$ can be different from C_y. (ii) The original non-Bloch Chern number defined in Eq. (13) is the physically more useful one. In fact, we find that wave-packet motions on the edges of cylinder follow the phase diagram of Fig. 1, namely, chiral edge motions are appreciable when C (instead of C_y) is nonzero. This is understandable because wave packets are quite ignorant of the periodic-boundary condition in the x direction if the cylinder circumference is much larger than the wave-packet size.

Conclusions.—We uncovered a non-Bloch bulk-boundary correspondence: the chiral edge states are determined by non-Bloch Chern numbers defined in the complex Brillouin zone. The obtained phase diagrams (also confirmed numerically) are qualitatively different from the Bloch-Hamiltonian counterparts. Our results suggest a non-Bloch framework for non-Hermitian band topology.

There are many open questions ahead. For example, it is worthwhile to study the respective roles of the Bloch and non-Bloch Chern numbers: what aspects of non-Hermitian physics are described by the Bloch or non-Bloch one? In addition, the theory can be generalized to many other topological non-Hermitian systems. It is also interesting to go beyond the band theory (e.g., to consider interaction effects).

We would like to thank Hui Zhai for discussions. This work is supported by NSFC under Grant No. 11674189.

*wangzhongemail@gmail.com

[1] C. M. Bender, Making sense of non-Hermitian Hamiltonians, Rep. Prog. Phys. **70**, 947 (2007).
[2] C. M. Bender and S. Boettcher, Real Spectra in Non-Hermitian Hamiltonians Having PT Symmetry, Phys. Rev. Lett. **80**, 5243 (1998).
[3] I. Rotter, A non-Hermitian Hamilton operator and the physics of open quantum systems, J. Phys. A Math Theor **42**, 153001 (2009).
[4] S. Malzard, C. Poli, and H. Schomerus, Topologically Protected Defect States in Open Photonic Systems with Non-Hermitian Charge-Conjugation and Parity-Time Symmetry, Phys. Rev. Lett. **115**, 200402 (2015).
[5] H. J. Carmichael, Quantum Trajectory Theory for Cascaded Open Systems, Phys. Rev. Lett. **70**, 2273 (1993).
[6] B. Zhen, C. W. Hsu, Y. Igarashi, L. Lu, I. Kaminer, A. Pick, S.-L. Chua, J. D. Joannopoulos, and M. Soljačić, Spawning rings of exceptional points out of dirac cones, Nature **525**, 354 (2015).
[7] S. Diehl, E. Rico, M. A. Baranov, and P. Zoller, Topology by dissipation in atomic quantum wires, Nat. Phys. **7**, 971 (2011).
[8] H. Cao and J. Wiersig, Dielectric microcavities: Model systems for wave chaos and non-Hermitian physics, Rev. Mod. Phys. **87**, 61 (2015).
[9] Y. Choi, S. Kang, S. Lim, W. Kim, J.-R. Kim, J.-H. Lee, and K. An, Quasieigenstate Coalescence in an Atom-Cavity Quantum Composite, Phys. Rev. Lett. **104**, 153601 (2010).
[10] P. San-Jose, J. Cayao, E. Prada, and R. Aguado, Majorana bound states from exceptional points in non-topological superconductors, Sci Rep **6**, 21427 (2016).
[11] T. E. Lee and C.-K. Chan, Heralded Magnetism in Non-Hermitian Atomic Systems, Phys. Rev. X **4**, 041001 (2014).
[12] T. E. Lee, F. Reiter, and N. Moiseyev, Entanglement and Spin Squeezing in Non-Hermitian Phase Transitions, Phys. Rev. Lett. **113**, 250401 (2014).
[13] K. G. Makris, R. El-Ganainy, D. N. Christodoulides, and Z. H. Musslimani, Beam Dynamics in $\mathcal{PT}$ Symmetric Optical Lattices, Phys. Rev. Lett. **100**, 103904 (2008).
[14] S. Longhi, Bloch Oscillations in Complex Crystals with $\mathcal{PT}$ Symmetry, Phys. Rev. Lett. **103**, 123601 (2009).
[15] C. E. Rüter, K. G. Makris, R. El-Ganainy, D. N. Christodoulides, M. Segev, and D. Kip, Observation of parity–time symmetry in optics, Nat. Phys. **6**, 192 (2010).
[16] S. Klaiman, U. Günther, and N. Moiseyev, Visualization of Branch Points in $\mathcal{PT}$-Symmetric Waveguides, Phys. Rev. Lett. **101**, 080402 (2008).
[17] S. Bittner, B. Dietz, U. Günther, H. L. Harney, M. Miski-Oglu, A. Richter, and F. Schäfer, PT-Symmetry and Spontaneous Symmetry Breaking in a Microwave Billiard, Phys. Rev. Lett. **108**, 024101 (2012).
[18] A. Regensburger, C. Bersch, M.-A. Miri, G. Onishchukov, D. N. Christodoulides, and U. Peschel, Parity–time synthetic photonic lattices, Nature **488**, 167 (2012).
[19] A. Guo, G. J. Salamo, D. Duchesne, R. Morandotti, M. Volatier-Ravat, V. Aimez, G. A. Siviloglou, and D. N. Christodoulides, Observation of $\mathcal{PT}$-Symmetry Breaking in Complex Optical Potentials, Phys. Rev. Lett. **103**, 093902 (2009).
[20] M. Liertzer, Li Ge, A. Cerjan, A. D. Stone, H. E. Türeci, and S. Rotter, Pump-Induced Exceptional Points in Lasers, Phys. Rev. Lett. **108**, 173901 (2012).
[21] B. Peng, Ş. K. Özdemir, S. Rotter, H. Yilmaz, M. Liertzer, F. Monifi, C. M. Bender, F. Nori, and L. Yang, Loss-induced suppression and revival of lasing, Science **346**, 328 (2014).

[22] Z. Lin, H. Ramezani, T. Eichelkraut, T. Kottos, H. Cao, and D. N. Christodoulides, Unidirectional Invisibility Induced by $\mathcal{PT}$-Symmetric Periodic Structures, Phys. Rev. Lett. **106**, 213901 (2011).

[23] L. Lu, J. D. Joannopoulos, and M. Soljacic, Topological photonics, Nat. Photonics **8**, 821 (2014).

[24] L. Feng, Y.-L. Xu, W. S. Fegadolli, M.-H. Lu, J. E. B. Oliveira, V. R. Almeida, Y.-F. Chen, and A. Scherer, Experimental demonstration of a unidirectional reflectionless parity-time metamaterial at optical frequencies, Nat. Mater. **12**, 108 (2013).

[25] R. Fleury, D. Sounas, and A. Alù, An invisible acoustic sensor based on parity-time symmetry, Nat. Commun. **6**, 5905 (2015).

[26] L. Chang, X. Jiang, S. Hua, C. Yang, J. Wen, L. Jiang, G. Li, G. Wang, and M. Xiao, Parity–time symmetry and variable optical isolation in active–passive-coupled microresonators, Nat. Photonics **8**, 524 (2014).

[27] H. Hodaei, A. U. Hassan, S. Wittek, H. Garcia-Gracia, R. El-Ganainy, D. N. Christodoulides, and M. Khajavikhan, Enhanced sensitivity at higher-order exceptional points, Nature **548**, 187 (2017).

[28] H. Hodaei, M.-A. Miri, M. Heinrich, D. N. Christodoulides, and M. Khajavikhan, Parity-time–symmetric microring lasers, Science **346**, 975 (2014).

[29] L. Feng, Z. J. Wong, R.-M. Ma, Y. Wang, and X. Zhang, Single-mode laser by parity-time symmetry breaking, Science **346**, 972 (2014).

[30] K. Kawabata, Y. Ashida, and M. Ueda, Information Retrieval and Criticality in Parity-Time-Symmetric Systems, Phys. Rev. Lett. **119**, 190401 (2017).

[31] T. Gao, E. Estrecho, K. Y. Bliokh, T. C. H. Liew, M. D. Fraser, S. Brodbeck, M. Kamp, C. Schneider, S. Höfling, Y. Yamamoto *et al.*, Observation of non-Hermitian degeneracies in a chaotic exciton-polariton billiard, Nature **526**, 554 (2015).

[32] H. Xu, D. Mason, L. Jiang, and J. G. E. Harris, Topological energy transfer in an optomechanical system with exceptional points, Nature **537**, 80 (2016).

[33] Y. Ashida, S. Furukawa, and M. Ueda, Parity-time-symmetric quantum critical phenomena, Nat. Commun. **8**, 15791 (2017).

[34] W. Chen, Ş. K. Özdemir, G. Zhao, J. Wiersig, and L. Yang, Exceptional points enhance sensing in an optical microcavity, Nature **548**, 192 (2017).

[35] K. Ding, G. Ma, M. Xiao, Z. Q. Zhang, and C. T. Chan, Emergence, Coalescence, and Topological Properties of Multiple Exceptional Points and Their Experimental Realization, Phys. Rev. X **6**, 021007 (2016).

[36] C. A. Downing and G. Weick, Topological collective plasmons in bipartite chains of metallic nanoparticles, Phys. Rev. B **95**, 125426 (2017).

[37] T. Ozawa, H. M. Price, A. Amo, N. Goldman, M. Hafezi, L. Lu, M. Rechtsman, D. Schuster, J. Simon, O. Zilberberg, and I. Carusotto, Topological photonics, arXiv:1802.04173.

[38] R. El-Ganainy, K. G. Makris, M. Khajavikhan, Z. H. Musslimani, S. Rotter, and D. N. Christodoulides, Non-Hermitian physics and PT symmetry, Nat. Phys. **14**, 11 (2018).

[39] S. Longhi, Parity-time symmetry meets photonics: A new twist in non-Hermitian optics, arXiv:1802.05025.

[40] V. Kozii and L. Fu, Non-Hermitian topological theory of finite-lifetime quasiparticles: Prediction of bulk fermi arc due to exceptional point, arXiv:1708.05841.

[41] M. Papaj, H. Isobe, and L. Fu, Bulk fermi arc of disordered dirac fermions in two dimensions, arXiv:1802.00443.

[42] H. Shen and L. Fu, Quantum Oscillation from In-Gap States and Non-Hermitian Landau Level Problem, Phys. Rev. Lett. **121**, 026403 (2018).

[43] H. Zhou, C. Peng, Y. Yoon, C. W. Hsu, K. A. Nelson, L. Fu, J. D. Joannopoulos, M. Soljačić, and B. Zhen, Observation of bulk fermi arc and polarization half charge from paired exceptional points, Science **359**, 1009 (2018).

[44] H. Shen, B. Zhen, and L. Fu, Topological Band Theory for Non-Hermitian Hamiltonians, Phys. Rev. Lett. **120**, 146402 (2018).

[45] K. Esaki, M. Sato, K. Hasebe, and M. Kohmoto, Edge states and topological phases in non-Hermitian systems, Phys. Rev. B **84**, 205128 (2011).

[46] T. E. Lee, Anomalous Edge State in a Non-Hermitian Lattice, Phys. Rev. Lett. **116**, 133903 (2016).

[47] D. Leykam, K. Y. Bliokh, C. Huang, Y. D. Chong, and F. Nori, Edge Modes, Degeneracies, and Topological Numbers in Non-Hermitian Systems, Phys. Rev. Lett. **118**, 040401 (2017).

[48] S. Lieu, Topological phases in the non-Hermitian Su-Schrieffer-Heeger model, Phys. Rev. B **97**, 045106 (2018).

[49] C. Yin, H. Jiang, L. Li, R. Lü, and S. Chen, Geometrical meaning of winding number and its characterization of topological phases in one-dimensional chiral non-hermitian systems, Phys. Rev. A **97**, 052115 (2018).

[50] H. Menke and M. M. Hirschmann, Topological quantum wires with balanced gain and loss, Phys. Rev. B **95**, 174506 (2017).

[51] M. S. Rudner and L. S. Levitov, Topological Transition in a Non-Hermitian Quantum Walk, Phys. Rev. Lett. **102**, 065703 (2009).

[52] C. Li, X. Z. Zhang, G. Zhang, and Z. Song, Topological phases in a Kitaev chain with imbalanced pairing, Phys. Rev. B **97**, 115436 (2018).

[53] Y. Xiong, Why does bulk boundary correspondence fail in some non-Hermitian topological models, arXiv:1705.06039v1.

[54] V. M. M. Alvarez, J. E. B. Vargas, and L. E. F. F. Torres, Non-Hermitian robust edge states in one dimension: Anomalous localization and eigenspace condensation at exceptional points, Phys. Rev. B **97**, 121401 (2018).

[55] Z. Gong, Y. Ashida, K. Kawabata, K. Takasan, S. Higashikawa, and M. Ueda, Topological phases of non-Hermitian systems, arXiv:1802.07964.

[56] S. Yao and Z. Wang, Edge States and Topological Invariants of Non-Hermitian Systems, Phys. Rev. Lett. **121**, 086803 (2018).

[57] S.-D. Liang and G.-Y. Huang, Topological invariance and global berry phase in non-Hermitian systems, Phys. Rev. A **87**, 012118 (2013).

[58] Y. C. Hu and T. L. Hughes, Absence of topological insulator phases in non-Hermitian *PT*-symmetric Hamiltonians, Phys. Rev. B **84**, 153101 (2011).

[59] J. Gong and Q.-h. Wang, Geometric phase in $\mathcal{PT}$-symmetric quantum mechanics, Phys. Rev. A **82**, 012103 (2010).

[60] M. S. Rudner, M. Levin, and L. S. Levitov, Survival, decay, and topological protection in non-Hermitian quantum transport, arXiv:1605.07652.

[61] B. Zhu, R. Lü, and S. Chen, $\mathcal{PT}$ symmetry in the non-Hermitian Su-Schrieffer-Heeger model with complex boundary potentials, Phys. Rev. A **89**, 062102 (2014).

[62] Z. Gong, S. Higashikawa, and M. Ueda, Zeno Hall Effect, Phys. Rev. Lett. **118**, 200401 (2017).

[63] X. Wang, T. Liu, Y. Xiong, and P. Tong, Spontaneous $\mathcal{PT}$-symmetry breaking in non-Hermitian Kitaev and extended Kitaev models, Phys. Rev. A **92**, 012116 (2015).

[64] K. Kawabata, Y. Ashida, H. Katsura, and M. Ueda, Parity-time-symmetric topological superconductor, Phy. Rev. B **98**, 085116 (2018).

[65] X. Ni, D. Smirnova, A. Poddubny, D. Leykam, Y. Chong, and A. B. Khanikaev, Exceptional points in topological edge spectrum of PT symmetric domain walls, arXiv: 1801.04689.

[66] A. A. Zyuzin and A. Y. Zyuzin, Flat band in disorder-driven non-Hermitian Weyl semimetals, Phys. Rev. B **97**, 041203 (2018).

[67] A. Cerjan, M. Xiao, L. Yuan, and S. Fan, Effects of non-Hermitian perturbations on Weyl Hamiltonians with arbitrary topological charges, Phys. Rev. B **97**, 075128 (2018).

[68] M. Klett, H. Cartarius, D. Dast, J. Main, and G. Wunner, Relation between $\mathcal{PT}$-symmetry breaking and topologically nontrivial phases in the Su-Schrieffer-Heeger and Kitaev models, Phys. Rev. A **95**, 053626 (2017).

[69] L. Zhou, Q.-h. Wang, H. Wang, and J. Gong, Dynamical quantum phase transitions in non-Hermitian lattices, Phys. Rev. A **98**, 022129 (2018).

[70] J. González and R. A. Molina, Topological protection from exceptional points in Weyl and nodal-line semimetals, Phys. Rev. B **96**, 045437 (2017).

[71] C. Yuce, Majorana edge modes with gain and loss, Phys. Rev. A **93**, 062130 (2016).

[72] W. Hu, H. Wang, P. P. Shum, and Y. D. Chong, Exceptional points in a non-Hermitian topological pump, Phys. Rev. B **95**, 184306 (2017).

[73] Y. Xu, S.-T. Wang, and L.-M. Duan, Weyl Exceptional Rings in a Three-Dimensional Dissipative Cold Atomic Gas, Phys. Rev. Lett. **118**, 045701 (2017).

[74] S. Ke, B. Wang, H. Long, K. Wang, and P. Lu, Topological edge modes in non-Hermitian plasmonic waveguide arrays, Opt. Express **25**, 11132 (2017).

[75] G. Harari, M. A. Bandres, Y. Lumer, M. C. Rechtsman, Y. D. Chong, M. Khajavikhan, D. N. Christodoulides, and M. Segev, Topological insulator laser: Theory, Science **359**, eaar4003 (2018).

[76] J. M. Zeuner, M. C. Rechtsman, Y. Plotnik, Y. Lumer, S. Nolte, M. S. Rudner, M. Segev, and A. Szameit, Observation of a Topological Transition in the Bulk of a Non-Hermitian System, Phys. Rev. Lett. **115**, 040402 (2015).

[77] L. Xiao, X. Zhan, Z. H. Bian, K. K. Wang, X. Zhang, X. P. Wang, J. Li, K. Mochizuki, D. Kim, N. Kawakami, W. Yi, H. Obuse, B. C. Sanders, and P. Xue, Observation of topological edge states in parity–time-symmetric quantum walks, Nat. Phys. **13**, 1117 (2017).

[78] S. Weimann, M. Kremer, Y. Plotnik, Y. Lumer, S. Nolte, K. G. Makris, M. Segev, M. C. Rechtsman, and A. Szameit, Topologically protected bound states in photonic parity–time-symmetric crystals, Nat. Mater. **16**, 433 (2017).

[79] C. Poli, M. Bellec, U. Kuhl, F. Mortessagne, and H. Schomerus, Selective enhancement of topologically induced interface states in a dielectric resonator chain, Nat. Commun. **6**, 6710 (2015).

[80] M. Parto, S. Wittek, H. Hodaei, G. Harari, M. A. Bandres, J. Ren, M. C. Rechtsman, M. Segev, D. N. Christodoulides, and M. Khajavikhan, Complex Edge-State Phase Transitions in 1D Topological Laser Arrays, Phys. Rev. Lett. **120**, 113901 (2018).

[81] H. Zhao, P. Miao, M. H. Teimourpour, S. Malzard, R. El-Ganainy, H. Schomerus, and L. Feng, Topological hybrid silicon microlasers, Nat. Commun. **9**, 981 (2018).

[82] X. Zhan, L. Xiao, Z. Bian, K. Wang, X. Qiu, B. C. Sanders, W. Yi, and P. Xue, Detecting Topological Invariants in Nonunitary Discrete-Time Quantum Walks, Phys. Rev. Lett. **119**, 130501 (2017).

[83] M. Z. Hasan and C. L. Kane, Colloquium: Topological insulators, Rev. Mod. Phys. **82**, 3045 (2010).

[84] X.-L. Qi and S.-C. Zhang, Topological insulators and superconductors, Rev. Mod. Phys. **83**, 1057 (2011).

[85] C.-K. Chiu, J. C. Y. Teo, A. P. Schnyder, and S. Ryu, Classification of topological quantum matter with symmetries, Rev. Mod. Phys. **88**, 035005 (2016).

[86] B. A. Bernevig and T. L Hughes, *Topological Insulators and Topological Superconductors* (Princeton University Press, Princeton, NJ, 2013).

[87] D. J. Thouless, M. Kohmoto, M. P. Nightingale, and M. den Nijs, Quantized Hall Conductance in a Two-Dimensional Periodic Potential, Phys. Rev. Lett. **49**, 405 (1982).

[88] F. D. M. Haldane, Model for a Quantum Hall Effect without Landau Levels: Condensed-Matter Realization of the "Parity Anomaly, Phys. Rev. Lett. **61**, 2015 (1988).

[89] C.-Z. Chang, J. Zhang, X. Feng, J. Shen, Z. Zhang, M. Guo, K. Li, Y. Ou, P. Wei, L.-L. Wang *et al.*, Experimental observation of the quantum anomalous hall effect in a magnetic topological insulator, Science **340**, 167 (2013).

[90] Z. Wang, Y. Chong, J. D. Joannopoulos, and M. Soljačić, Observation of unidirectional backscattering-immune topological electromagnetic states, Nature **461**, 772 (2009).

[91] M. A. Bandres, S. Wittek, G. Harari, M. Parto, J. Ren, M. Segev, D. N. Christodoulides, and M. Khajavikhan, Topological insulator laser: Experiments, Science **359**, eaar4005 (2018).

[92] X. L. Qi, Y. S. Wu, and S. C. Zhang, Topological quantization of the spin hall effect in two-dimensional paramagnetic semiconductors, Phys. Rev. B **74**, 085308 (2006).

[93] T. D. Lee and C. N. Yang, Statistical theory of equations of state and phase transitions. II. Lattice gas and Ising model, Phys. Rev. **87**, 410 (1952).

[94] A. Mostafazadeh, Pseudo-hermiticity versus PT symmetry: The necessary condition for the reality of the spectrum of a non-Hermitian Hamiltonian, J. Math. Phys. (N.Y.) **43**, 205 (2002).

[95] A. Mostafazadeh, Pseudo-hermiticity versus PT-symmetry. II. A complete characterization of non-Hermitian Hamiltonians with a real spectrum, J. Math. Phys. (N.Y.) **43**, 2814 (2002).

[96] The gap in $L \to \infty$ limit is determined from the intercept in the gap^2-$1/L^2$ plot.

[97] See Supplemental Material at http://link.aps.org/supplemental/10.1103/PhysRevLett.121.136802 for details of calculations.

[98] It remains meaningful to talk about "bulk eigenstates" because their number grows as L^2.

[99] In 1D non-Hermitian SSH models, a similar phenomenon has been seen numerically [54] and analytically [56]. Our 2D model establishes that this phenomenon is not merely a peculiar 1D effect, but a general feature of non-Hermitian bands.

[100] Exponential localization is also confirmed numerically (see the Supplemental Material [97]).

[101] For example, the non-Bloch Chern number of $H(\mathbf{k}) = \sum_{j=x,y} \sin(k_j + i\gamma_j)\sigma_j + [m - t\sum_j \cos(k_j + i\gamma_j)]\sigma_z$ jumps from 1 to 0 at $m = 2t$ (independent of the value of $\gamma_{x,y}$) (see the Supplemental Material [97]).